



Defect-rich one-dimensional MoS₂ hierarchical architecture for efficient hydrogen evolution: Coupling of multiple advantages into one catalyst



Shilong Jiao^a, Zhaoyu Yao^b, Fei Xue^c, Yangfan Lu^d, Maochang Liu^c, Huiqiu Deng^e, Xiufang Ma^a, Zhixiao Liu^{b, **}, Chao Ma^b, Hongwen Huang^{b,d,*}, Shuangchen Ruan^a, Yu-Jia Zeng^{a, **}

^a College of Physics and Optoelectronic Engineering, Shenzhen University, Shenzhen, 518060, PR China

^b College of Materials Science and Engineering, Hunan University, Changsha, Hunan, 410082, PR China

^c International Research Center for Renewable Energy, State Key Laboratory of Multiphase Flow in Power Engineering, Xi'an Jiaotong University, Xi'an, Shaanxi, 710049, PR China

^d State Key Lab of Silicon Materials, School of Materials Science and Engineering, Zhejiang University, Hangzhou, 310027, PR China

^e School of Physics and Electronics, Hunan University, Changsha, Hunan 410082, PR China

ARTICLE INFO

Keywords:

Hydrogen evolution reaction
MoS₂
Defect engineering
Coupling effect
Vacancy

ABSTRACT

Optimizing the activity of layered molybdenum disulfide (MoS₂) toward hydrogen evolution reaction (HER) process is generally achieved by improving the electrical transport, intrinsic activity, and/or the number of active sites. However, simultaneously coupling these factors to achieve remarkable MoS₂-based electrocatalysts has been seldom reported. Herein, we report a facile approach to the defect-rich one-dimensional MoS₂ hierarchical architecture (1D-DRHA MoS₂), which synergistically integrate the advantageous structural features of rich defects and one-dimensional hierarchical morphology. Toward HER process, the 1D-DRHA MoS₂ electrocatalyst exhibited an overpotential of 119 mV at 10 mA cm⁻², a Tafel slope of 50.7 mV dec⁻¹, accompanied by an excellent stability. Notably, the activity is competitive to the state-of-the-art MoS₂-based electrocatalysts for HER. The combination of experimental evidences and density functional theory calculations demonstrated the incorporation of rich defects and one-dimensional hierarchical structure improved electric conductivity, intrinsic activity, and active sites, which together accounted for the boosted HER performance.

1. Introduction

Hydrogen has been regarded as the next-generation energy carrier due to the zero-pollution emission and ultrahigh energy density [1–4]. Electrochemical water splitting powered by renewable electricity offers a promising approach for the sustainable production of hydrogen [5,6]. Noble-metal based electrocatalysts, particularly for Pt-based electrocatalysts, show excellent performance toward hydrogen evolution reaction (HER) owing to the high exchange current density and small overpotentials [7]. However, the large-scale deployment of this technique has been largely prohibited by its high cost. Great efforts have therefore been devoted to the replacement of precious Pt with earth-abundant materials, mainly including the transition metal carbides, sulfides, borides, nitrides, and phosphides [7–12].

Recently, two-dimensional layered molybdenum disulfide (MoS₂) has been intensively investigated as a promising alternative to Pt-based electrocatalyst owing to the analogous hydrogen adsorption energy and

excellent stability in both alkaline and acidic electrolytes [2,7]. Unfortunately, the catalytic kinetics of MoS₂ catalyst toward HER are generally limited by the low density of active sites arising from the large proportion of inactive basal planes in nanostructured MoS₂, as well as the undesirable electron transfer ability due to the semiconductor feature of common 2H-MoS₂ [13]. To boost the number of active sites, activating the MoS₂ basal plane and maximizing the exposing edge sites represent two general strategies, which can be achieved by engineering the phase, modulating the strain, creating the sulfur vacancies, doping the heteroatoms, forming unique microstructures, and so on [14–21]. It should be noted that the strategies to increase the active sites usually positively impact the intrinsic activity of MoS₂ via optimizing the hydrogen adsorption energy, offering a two-fold benefits [1,22]. As for the improvement of electrical conductivity, hybridization of MoS₂ with highly conductive carbon, formation of hierarchical structure, and preparation of metallic 1T-MoS₂ represent the powerful methods [16,20,21,23–26]. Despite the great progress that

* Corresponding author at: College of Materials Science and Engineering, Hunan University, Changsha, Hunan, 410082, PR China

** Corresponding author.

E-mail addresses: zxliu@hnu.edu.cn (Z. Liu), huanghw@hnu.edu.cn (H. Huang), yjzeng@szu.edu.cn (Y.-J. Zeng).

has been made, the design of efficient MoS₂ catalyst by simultaneously optimizing the number of active sites, intrinsic activity, and electric conductivity has been seldom and is highly desirable.

Herein, we report the synthesis of defect-rich one-dimensional hierarchical MoS₂ architecture (1D-DRHA MoS₂), which exhibits multiple structural advantages. On the nanoscale level, assembled hierarchical architecture remarkably strengthened the electron transportation and charge transfer process. On the atomic level, the rich sulfur vacancies activated the basal plane of 1D-DRHA MoS₂, thus largely increasing the number of active sites. Besides, the theoretical calculations indicated that the presence of sulfur vacancies optimized the hydrogen adsorption free energy ΔG_H , causing the improved intrinsic activity of the active centers. Coupling of these advantages together, the achieved 1D-DRHA MoS₂ electrocatalyst exhibited a remarkable activity and an excellent stability toward HER process.

2. Experimental section

2.1. Synthesis of the one-dimensional MoS₂ hierarchical architecture (1D-HA MoS₂)

The 1D-HA MoS₂ was prepared via the hydrothermal method. In a typical process, 4 mmol Na₂MoO₄ and 15 mmol thioacetamide were added into the mixture of 10 ml ethanol and 20 ml oleic acid, and then the solution was stirred for 30 min. The solution was then transferred into a 40 ml Teflon tube and sealed into the autoclave, which was heated to 240 °C for 24 h. The obtained products were washed several times with ethanol and water after cooling to the room temperature. Finally, they were dried at 60 °C for 12 h for further characterization. To investigate the growth process of the MoS₂ super structure, time-dependent experiments were carried out for 4, 8, 12 and 24 h, respectively. Additionally, the effect of Mo source on the product morphology was also examined by substituting Na₂MoO₄ with molybdic acid, ammonium molybdate, molybdenum trichloride and molybdenum (V) chloride. The ratio of the oleic acid and ethanol was investigated by changing the volume ration between them to 1:14, 1:5, 1:1 and 5:1.

2.2. Synthesis of the defect-rich one-dimensional MoS₂ hierarchical architecture (1D-DRHA MoS₂)

The 1D-DRHA MoS₂ was obtained via a simple solution method by treating the sample with 0.1 mol L⁻¹ (in ethanol) NaBH₄. Typically, 10 mg as-obtained 1D-HA MoS₂ was added into 4 ml ethanol and was sonicated for 30 min to get a homogeneous solution, then 6 ml 0.1 mol L⁻¹ NaBH₄ was added to get a concentration of 1 mg_{MoS2}/mL. The solution was further sonicated for 2 h to get the final product. The obtained products were washed several times with ethanol and water after cooling to the room temperature. Finally, they were dried at 60 °C for 12 h for further characterization.

2.3. Electrochemical measurements

All electrochemical measurements were carried out at room temperature with a standard three-electrode cell system, which was connected to an electrochemical workstation (CHI 660E, Chenhua, Shanghai, China). A piece of paper (1 × 1 cm²) loaded with catalysts on one side acted as the working electrode and the Ag/AgCl and a graphite rod acted as reference and counter electrodes, respectively. The catalyst ink was prepared by dispersing 4 mg catalyst into 0.4 ml ethanol containing 20 µl of 5 wt% Nafion solution followed by 1 h sonication in the water bath. The working electrode was prepared by drop-casting 100 µl of ink onto the carbon paper and dried at room temperature prior to the electrochemical measurements. HER tests were conducted in N₂-saturated 0.5 M H₂SO₄ electrolyte at room temperature. The LSV (Linear Sweep Voltammetry) curves were collected with a scan rate of 3 mV s⁻¹ from 0 to -0.5 V (vs. RHE). Cyclic voltammetry (CV) was conducted to

evaluate catalyst stability by performing 1000 cycles. ECSA was estimated by CV cycling from 0.4 – 0.8 V (vs. RHE) in 0.5 M H₂SO₄ at sweep rates of 10 – 100 mV s⁻¹. Since the capacitance of an ideally smooth electrode in acidic media is usually taken as 35 µF cm⁻², ECSA was estimated using the equation: $A_{ECSA} = C_{dl} / (35 \mu F cm^{-2} per cm^2_{ECSA})$. All the polarization curves were obtained without iR compensation.

2.4. Calculation of TOFs

The turnover frequency is defined as the number of turnovers per active site per second. The TOF in this study was calculated using the following formula:

$$TOF$$

$$= \left(j \frac{mA}{cm^2} \right) \left(\frac{1 C s^{-1}}{1000 mA} \right) \left(\frac{1 mol e^-}{96485 C} \right) \left(\frac{1 mol H_2}{2 mol e^-} \right) \left(\frac{6.02 \times 10^{23} H_2 molecules}{1 mol H_2} \right)$$

$$= 3.12 \times 10^{15} \frac{H_2/s}{cm^2 per cm^2}$$

For MoS₂, the active site per real surface are obtained from the unit cell of the MoS₂:

$$active sites = \left(\frac{atoms/unit cell}{Volume/unit cell} \right)^{\frac{2}{3}}$$

As it was obviously known that the unit cell of MoS₂ contained one Mo atom and two S atoms with a volume of 53.1 Å³. From that the calculated active sites for the electrocatalysts is 1.12×10^{15} atoms cm⁻². Based on the above-mentioned results, the TOF value can be described as follows:

$$TOF = \frac{\left(3.12 \times 10^{15} \frac{H_2/s}{cm^2 per cm^2} \right) \times j}{active sites \times ECSA}$$

Note that the calculated TOF values should be smaller than the real value since we considered all the surface area rather than the edge sites of the electrocatalysts.

2.5. DFT calculation details

The Gibbs energy diagram was calculated by

$$\Delta G = G_{H/MoS_2} - G_{MoS_2} - \frac{1}{2}\mu_{H_2} \quad (1)$$

$$G = E + H^{vib} - TS^{vib} \quad (2)$$

Here E is the potential energy calculated by the first-principles approach at 0 K. H^{vib} is the enthalpy contributed by the atom vibration:

$$H^{vib} = \sum i\hbar\omega_i \left(\frac{1}{2} + \left(\exp\left(\frac{\hbar\omega_i}{\kappa T}\right) - 1 \right)^{-1} \right) \quad (3)$$

S^{vib} is the vibrational entropy:

$$S^{vib} = \sum i\kappa \left(\frac{\hbar\omega_i}{\kappa T} \left(\exp\left(\frac{\hbar\omega_i}{\kappa T}\right) - 1 \right)^{-1} - \ln\left(1 - \exp\left(-\frac{\hbar\omega_i}{\kappa T}\right)\right) \right) \quad (4)$$

In Eqt. 1, G_{H/MoS_2} is the Gibbs energy of the system with a H atom adsorbed on the MoS₂ substrate, G_{MoS_2} is the Gibbs energy of the clean substrate, and μ_{H_2} is the chemical potential of a H₂ molecule.

2.6. Material characterizations

High-resolution high-angle annular dark-field scanning transmission electron microscopy (HAADF-STEM) and tomography images were carried out on a Cs-corrected FEI Titan 80/300 kV TEM/STEM microscope at ORNL. Powder X-ray diffraction (XRD) patterns were recorded using an X-ray diffractometer (SmartLab (3), Rigaku) operated at 3 kW.

X-ray photoelectron spectroscopy (XPS) analyses were performed using a Kratos Ultra DLD spectrometer equipped with monochromatic Al K radiation. The binding-energy scales were calibrated using the C1s peak at 284.6 eV, resulting from C contamination. Morphologies of the samples were examined with transmission electron microscope (TEM, JEOL H-7000). Raman measurements were performed in backscattering geometry at room temperature using a confocal Raman spectroscopy set up (NTEGRANTMDT) using a 532 nm laser. The electron paramagnetic resonance (EPR) spectra were detected on a Bruker EPR spectrometer. The Accelerated Surface Area and Porosimeter 2000 analyzer was used to measure the Brunauer – Emmett – Teller (BET) specific surface area of the sample.

3. Results and discussion

The schematic illustration for the preparation of one-dimensional defect-rich MoS₂ hierarchical architecture (denoted as 1D-DRHA MoS₂ for convenience) is shown in Fig. S1a. In the first step, the pristine one-dimensional MoS₂ hierarchical architecture (denoted as 1D-HA MoS₂ for convenience) were obtained via a solvothermal synthesis, in which sodium molybdate dehydrate (Na₂MoO₄·2H₂O) and thioacetamide (CH₃C_{SNH}₂) were used as Mo and S sources, respectively, oleic acid and ethanol were used as surfactant and solvent (see details in Experimental Section). Afterwards, the 1D-DRHA MoS₂ were prepared by treating the 1D-HA MoS₂ with NaBH₄ aqueous solution.

The representative transmission electron microscopy (TEM) images clearly show that the morphological structure of the pristine products are one-dimensional hierarchical architecture with subunits consisting of lamellar nanosheets (Fig. S1b-c). The powder XRD indicates the production of MoS₂ 2H-phase (Fig. S2), suggesting the formation of 1D-HA MoS₂. The formation process of the 1D-HA MoS₂ was also clearly traced by characterizing the obtained intermediates at different reaction stages. As shown in Fig. S3a, only amorphous products can be obtained at 4 h. By prolonging the reaction time, the amorphous products evolved into three-dimensional hierarchical nanoflowers consisting of lamellar nanosheets (Fig. S3b). The three-dimensional hierarchical nanoflowers (3D-HNF) further assembled into one-dimensional hierarchical architecture with lamellar nanosheets as subunits as the reaction time extended to 12 and 24 h (Fig. S3c and Fig. S3d). The driving force for such morphological evolution is probably stemmed from the minimization of the surface energy [27–29]. Note that there was no phase change during the morphological evolution from three-dimensional MoS₂ hierarchical nanoflowers to one-dimensional MoS₂ hierarchical architecture, as indicated by the XRD patterns of the products obtained at different reaction stages (Fig. S4). In addition, the impacts of the precursors and ratio of oleic acid to ethanol were also studied to gain the insights into the successful synthesis of 1D-HA MoS₂ (Fig. S5 and Fig. S6). The results indicated that the Mo precursor and ratio of oleic acid to ethanol could greatly influence the morphology of products, which can be rationalized from the point view of reaction thermodynamics and kinetics.

The 1D-DRHA MoS₂ was then obtained by treating the 1D-HA MoS₂ with NaBH₄ solution. The structure of as-prepared products was then carefully examined. Fig. 1a demonstrates that the morphology of the products retained the structure of 1D-HA MoS₂, with the characteristic of one-dimensional hierarchical nanostructure consisting of lamellar subunits. Such one-dimensional hierarchical architecture exhibits an average diameter of 100 nm and a length of several hundred nanometers (more than 500 nm). The detailed structural information of the hierarchical architecture is further revealed by HAADF-STEM. As shown in Fig. 1b, the high-magnification HAADF-STEM image confirms that the lamellar nanosheets are the subunits of hierarchical architecture. The interlayer spacing of the lamellar subunit is determined to be of 0.63 nm, corresponding to the (002) lattice plane of the 2H-MoS₂ (Fig. 1c). Moreover, such hierarchical structure with lamellar nanosheets as subunits allows the exposure of a large fraction of active

edge sites, which is believed to facilitate the kinetics of HER [30]. Fig. 1d shows the atomic-resolution HAADF-STEM image recorded from the basal plane of the lamellar nanosheets. The atomic arrangements of Mo and S atoms observed from the image, as well as the intensity profile recorded as marked by the lines in Fig. 1d, both verify the phase of 2H-MoS₂ (Fig. 1e and L1-2 in Fig. 1f), consistent with the XRD results. In addition, high-density defects including the sulfur vacancies, distorted lattice and Mo-edged sites, can be evidently observed on the basal plane (Fig. 1d-e), which have been previously reported to activate the basal plane of 2H-MoS₂ for efficient HER process [13,31–33]. The corresponding intensity profile recorded also demonstrates the irregular arrangement and the existence of the atomic defects in the 1D-DRHA (L3 in Fig. 1f). The corresponding elemental mapping images of the prepared hierarchical MoS₂ structure reveal that the Mo and S are uniformly distributed (Fig. 1g-i). The atomic ratio of S/Mo is estimated as 1.85 based on the energy-dispersive spectroscopy (EDS) analysis, implying the sulfur deficiency in the hierarchical structure.

The presence of sulfur vacancies was further testified by a combination of XPS, EPR spectra and Raman spectroscopy techniques. Fig. 2a shows the XPS spectra of Mo 3d regions. The binding energies at 229.4 and 232.5 eV are assigned to Mo 3d_{5/2} and Mo 3d_{3/2}, respectively, indicating the existence of Mo⁴⁺. The binding energies at 162.8 and 163.9 eV are indexed to S 2p_{3/2} and S 2p_{1/2}, respectively, consistent with S²⁻ (Fig. 2b). In comparison with 1D-HA MoS₂, the Mo 3d and S 2p peaks of 1D-DRHA MoS₂ exhibits obvious negative shifts of ~0.7 and ~0.9 eV, respectively. Such negative shifts, consistent with the previous reports, hints the presence of sulfur vacancies, which is also substantiated by the decreased atomic ratio of S/Mo from 1.96 to 1.83 as compared to the 1D-HA MoS₂ [13,15]. Notably, the decreased binding energies of Mo 3d and S 2p peaks for 1D-DRHA MoS₂ reflects the characteristic of electron-rich surface, which represents the optimized electronic structure of MoS₂ by promoting the proton adsorption for the HER process [19,30,34]. The paramagnetic signals were detected by measuring the unpaired electrons on coordinatively unsaturated defective sites using EPR to reveal the information of sulfur vacancies for 1D-HA MoS₂ and 1D-DRHA MoS₂. As shown in Fig. 2c, both samples exhibits a signal at g = 2.02 that arises from the sulfur vacancy [35–37]. Moreover, the amplified and broadened signal of the 1D-DRHA MoS₂ indicates the increased concentration of sulfur vacancies [15,33]. The Raman spectra of the 1D-HA MoS₂ and 1D-DRHA MoS₂ are displayed in Fig. 2d. The peaks at ~380 and ~405 cm⁻¹ are assigned to the in-plane Mo-S phonon mode (E_{2g}¹) excited by terrace-terminated MoS₂ layer and out-of-plane Mo-S phonon mode (A_{1g}) excited by edge-terminated MoS₂ layer, respectively [38–40]. As the peak intensity ratio of E_{2g}¹ and A_{1g} can indicate the edge-exposed degree of MoS₂ and a smaller value implies high edge exposure degree, the 1D-DRHA MoS₂ shows a much lower E_{2g}¹/A_{1g} value compared to 1D-HA MoS₂ and thus a much higher fraction of exposed edge sites [33]. The increased exposed active edge sites are related with the generation of defect-rich structure, which create more coordinatively unsaturated edge sites. Due to the combination of optimized electronic structure and increased exposed active edge sites, such 1D-DRHA MoS₂ is expected to substantially accelerate the catalytic kinetics of HER process.

The electrocatalytic performance of the 1D-DRHA MoS₂ toward HER was then evaluated in 0.5 M H₂SO₄ aqueous solution using a standard three-electrode system (without iR correction), with 1D-HA MoS₂, 3D-HNF MoS₂, commercial MoS₂ nanoparticles, and commercial Pt/C as reference catalysts. Fig. 3a shows the representative linear sweep voltammograms (LSVs) recorded from different electrocatalysts for HER. Obviously, 1D-DRHA MoS₂ electrocatalyst shows the highest HER activity among of all MoS₂-based electrocatalysts. The detailed observations with the subtraction of the capacitive current density in Fig. 3b indicate that 1D-DRHA MoS₂ electrocatalyst exhibits an overpotential of 10 mA cm⁻² at only 119 mV, much lower than those of 1D-HA MoS₂ electrocatalyst (10 mA cm⁻² at 146 mV), 3D-HNF MoS₂ (10 mA cm⁻² at 155 mV), commercial MoS₂ nanoparticles (10 mA

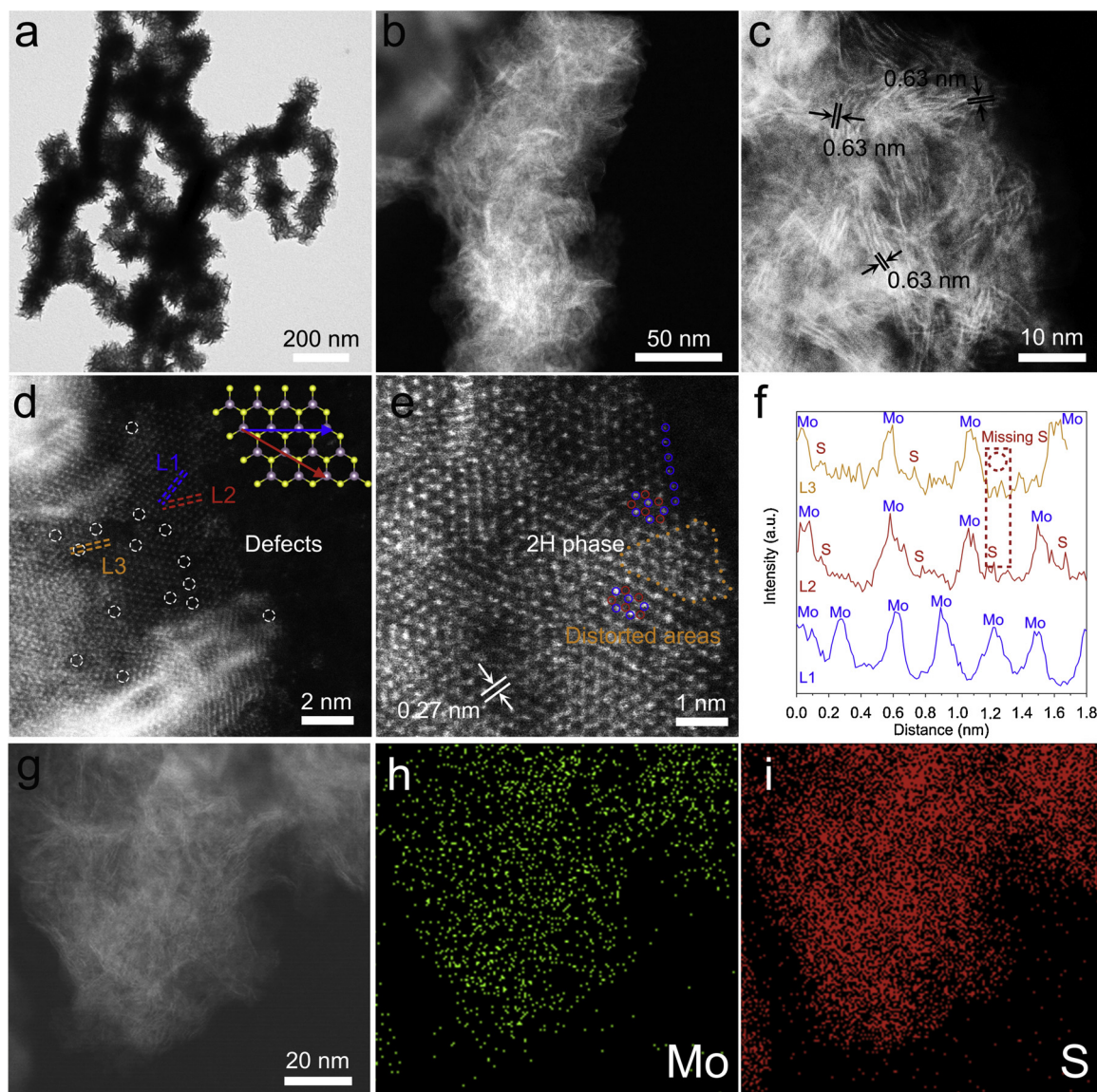


Fig. 1. Structural characterizations. (a) Low-magnification TEM image of the 1D-DRHA MoS₂. (b) Low-magnification HAADF-STEM image of the 1D-DRHA MoS₂. (c) High-magnification HAADF-STEM image of the 1D-DRHA MoS₂ showing the inter-layer distance. (d) Atomic-resolution HAADF-STEM image of the 1D-DRHA MoS₂ with multiple defects. Inset shows the corresponding scan directions in MoS₂ atomic model. (e) Atomic-resolution HAADF-STEM image of the 1D-DRHA MoS₂ showing the distorted areas and Mo-edged sites. (f) The intensity profile recorded from panel (d) along the lines. (g-i) EDX elemental mapping for the 1D-DRHA MoS₂.

cm⁻² at 179 mV). It should be noted that such low overpotential of 1D-DRHA MoS₂ electrocatalyst is comparable to the reported most active MoS₂-based non-precious HER electrocatalysts in acidic medium (Fig. S7 and Table S1). The rate-determining step (RDS) and the HER kinetics were further revealed by the Tafel plots derived from the corresponding LSV curves, as depicted in Fig. 3c. The 1D-DRHA MoS₂ electrocatalyst shows a Tafel slope of 50.7 mV dec⁻¹, whereas 1D-HA MoS₂, 3D-HNF MoS₂ and commercial MoS₂ nanoparticles electrocatalysts exhibit the Tafel slopes of 120, 206 and 230 mV dec⁻¹, respectively. As it indicated that the introduction of sulfur defects into the one-dimensional hierarchical structure could change the RDS from the Volmer step to the electrochemical desorption step [41]. Besides, the exchange current densities (J_o), an indicator reflecting the kinetics of charge transfer reactions, is derived by extrapolating Tafel plots to 0 mV for the MoS₂-based electrocatalysts. Expectedly, the 1D-DRHA MoS₂ electrocatalyst shows a J_o value of 1.56 mA cm⁻², much higher than those of 1D-HA MoS₂ electrocatalyst (1.21 mA cm⁻²), 3D-HNF MoS₂ (0.98 mA cm⁻²) and commercial MoS₂ nanoparticles (0.89 mA cm⁻²). Another

fundamental kinetic parameter, namely the turnover frequency (TOF), was also investigated. The calculated TOF values at the overpotential of 300 mV for the 1D-DRHA MoS₂ is 2.38 H₂ s⁻¹, which is much higher than that of the 1D-HA MoS₂ (1.90 H₂ s⁻¹), 3D-HNF MoS₂ (1.75 H₂ s⁻¹) and the commercial MoS₂ (0.18 H₂ s⁻¹), as displayed in Fig. S8. Taken together, the lowest overpotential, smallest Tafel slope, as well as the highest J_o value and TOF value, explicitly demonstrated the highest catalytic activity of 1D-DRHA MoS₂ electrocatalyst for HER process.

Another important parameter for the evaluation of the performance of electrocatalyst is the catalytic stability. To investigate the durability of the 1D-DRHA MoS₂ electrocatalyst, long-term stability test at an overpotential of 200 mV was carried out. After 24 h cycling, the current density of the 1D-DRHA MoS₂ electrocatalyst remained stable, suggesting the great catalytic durability (Fig. S9). To further attest the excellent stability of the 1D-DRHA MoS₂ electrocatalyst during the HER process, consecutive LSV scans are operated (Fig. 3d). The LSV curves show very small shift and only ~11 mV of degradation at the current density of 10 mA cm⁻² (inset of Fig. 3d), demonstrating the excellent

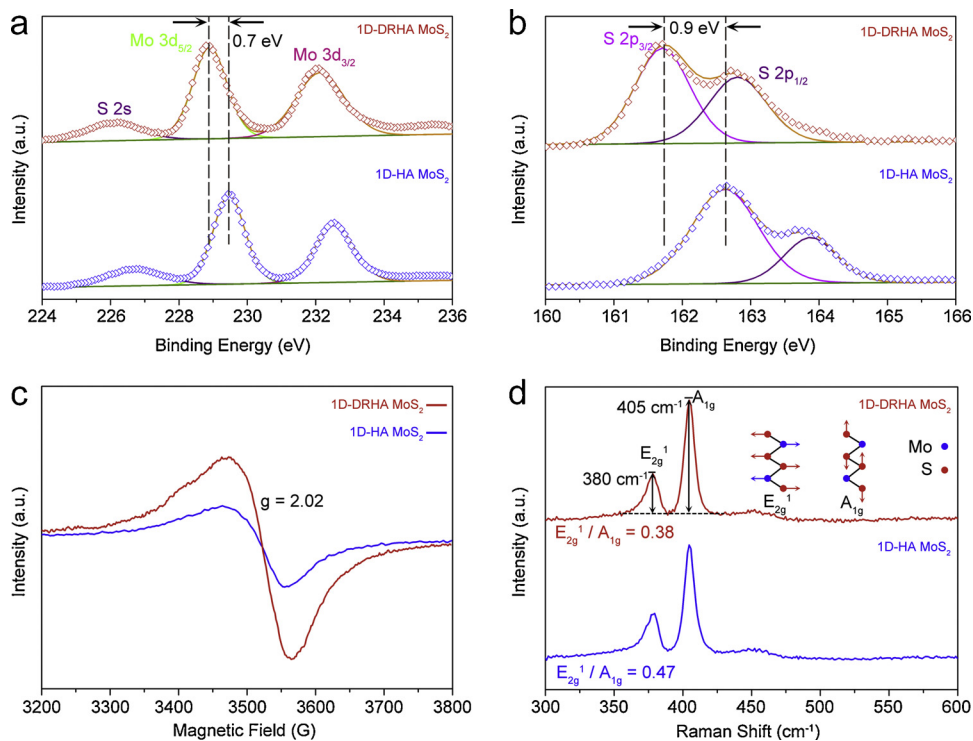


Fig. 2. Evidences of rich defects. (a, b) Mo 3d and S 2p XPS spectra of the 1D-DRHA MoS₂ and the 1D-HA MoS₂. (c, d) EPR patterns and the Raman spectra of the 1D-DRHA MoS₂ and the 1D-HA MoS₂.

stability of the electrocatalyst again, which is consistent with the morphology and composition characterizations of the 1D-DRHA MoS₂ after the stability test (Figure S10).

Given the detailed structural characterizations and the corresponding HER performance, the origin of the good catalytic activity of the 1D-DRHA MoS₂ electrocatalyst can be reasonably attributed to the integration of abundant defects and one-dimensional morphological

structure. We then focused on understanding how the features of defect and one-dimensional morphological structure of MoS₂ improved the HER kinetics. The electrochemically active surface areas (ECSA) were calculated to reveal the number of active sites by measuring the double-layer capacitance (C_{dl}). The value of C_{dl} for 1D-DRHA MoS₂ electrocatalyst is 6.93 mF cm⁻², which is higher than those of the 1D-HA MoS₂ electrocatalyst (3.84 mF cm⁻²), 3D-HNF MoS₂ electrocatalyst

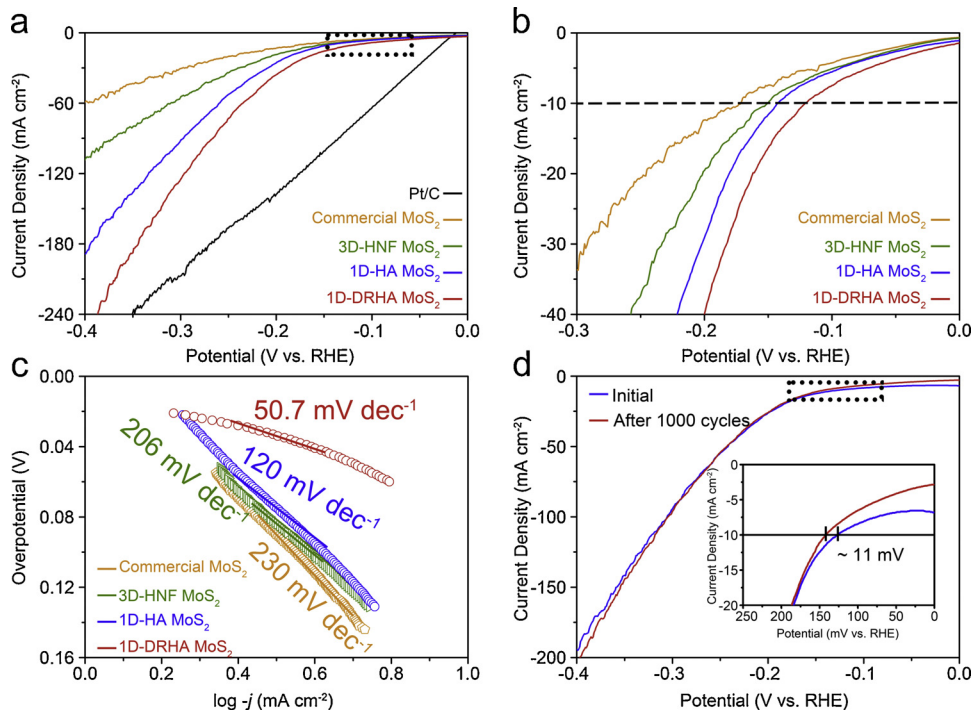


Fig. 3. Electrocatalytic performance for HER. (a) Polarization curves of different electrocatalysts. (b) The plot showing the curves marked in panel (a). (c) Tafel slopes of different electrocatalysts. (d) The LSVs of the 1D-DRHA MoS₂ before and after 1000 cycles.

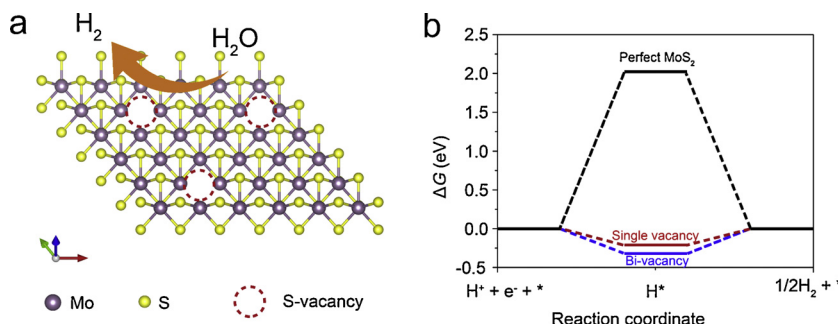


Fig. 4. DFT calculations. (a) Schematic of the top views of MoS₂ with S-vacancies on the basal plane. (b) Diagram of Gibbs free energy for HER on perfect and defect-rich 2H-MoS₂ surface.

(1.65 m F cm⁻²) and commercial MoS₂ electrocatalyst (0.96 m F cm⁻²) (Fig. S11 and Fig. S12). The trends in values of C_{dl} for different electrocatalysts are also supported by the trends in the values of Brunauer–Emmett–Teller (BET) surface area (Fig. S13). The largest ECSA value of 1D-DRHA MoS₂ electrocatalyst indicates the maximum number of active sites, which partially contributes to the fastest catalytic kinetics. The reason for the increased ECSA may be attributed to the presence of defect-rich structure, which was previously reported to activate the basal plane sites [13].

Density functional theory (DFT) calculations were performed to gain the insights into the role of sulfur vacancy, the predominant defect in the 1D-DRHA MoS₂ electrocatalyst, in HER kinetics from point view of electronic structure and adsorption strength of key intermediates (Fig. 4a and Fig. S14). To more accurately simulate the catalyst, effects of single vacancy and bi-vacancy clusters were considered in the present study. As shown in Fig. 4b, the Gibbs reaction energy for H⁺ reduces to H on the perfect 2H-MoS₂ is higher than 2 eV, which indicates that the reaction is not thermodynamically allowed. By contrast, it can be found that both single vacancy and bi-vacancy cluster leads to a negative Gibbs reaction energy. Given that vacancies are the active catalytic site for HER, the reduced H has to detach from the active site as soon as possible to activate following HER. Therefore, the vacancy should not provide a strong affinity the H atom. As shown in Fig. 4b, the Gibbs reaction energy of H adsorption on the single vacancy site is much closer to 0 eV. It can be inferred that single vacancies are preferred for catalyzing HER on MoS₂.

The positive impact of one-dimensional nanostructure on the HER kinetics can be concluded by comparing the HER performance of 1D-HA MoS₂ electrocatalyst and 3D-HNF MoS₂ electrocatalyst. It is believed that one-dimensional nanostructure provides an unblocked pathway for electron transfer relative to three-dimensional nanostructure. The electrical transport properties revealed by the electrochemical impedance spectrum (EIS) verifies that 1D-DRHA MoS₂ electrocatalyst exhibits much smaller charge-transfer resistance and higher charge-transportation property (Fig. S15). The improved electrical transport properties of 1D-DRHA MoS₂ electrocatalyst arising from one-dimensional nanostructure also partially accounted for the outstanding HER kinetics.

4. Conclusions

In summary, we presented a facile synthesis of the defective MoS₂ one-dimensional hierarchical architecture with enhanced HER performance by simultaneously tailoring the intrinsic activity, active site density and electrical transport property of the electrocatalyst. Owing to the multiple structural advantages, the as-prepared 1D-DRHA MoS₂ showed enhanced electrical transport property, intrinsic activity, and active sites. As a result, superior yet stable activity with a low overpotential of 119 mV at the current density of 10 mA cm⁻², a Tafel slope of 50.7 mV dec⁻¹, and excellent long-term stability was achieved. Such excellent HER activity makes it a low cost, efficient, robust and highly

competitive earth-abundant electrocatalysts for the hydrogen generation in the electrochemical water splitting, confirming its potential of replacing noble-metal catalyst. We believe the present work not only provides a marvelous HER electrocatalyst, but also offers a general concept to design efficient electrocatalysts.

Declaration of competing interest

The authors declare no competing financial interest.

Acknowledgements

This work was supported by the NSFC under Grant No. 21603208 and 51802092, the Shenzhen Science and Technology Project under Grant Nos. JCYJ20170412105400428 and JCYJ20180507182246321, the Shenzhen Peacock Technological Innovation Project under Grant No. KJQSCX20170727101208249, Fundamental Research Funds for the Central Universities, and the Open Project Program of the State Key Laboratory of Silicon Materials, Zhejiang University.

Appendix A. Supplementary data

Supplementary material related to this article can be found, in the online version, at doi:<https://doi.org/10.1016/j.apcatb.2019.117964>.

References

- [1] J. Ding, Y. Zhou, Y. Li, S. Guo, X. Huang, MoS₂ nanosheet assembling superstructure with a three-dimensional ion accessible site: a new class of bifunctional materials for batteries and electrocatalysis, *Chem. Mater.* 28 (2016) 2074–2080, <https://doi.org/10.1021/acsm.chemmater.5b04815>.
- [2] Q. Ding, B. Song, P. Xu, S. Jin, Efficient electrocatalytic and photoelectrochemical hydrogen generation using MoS₂ and related compounds, *Chem.* 1 (2016) 699–726, <https://doi.org/10.1016/j.chempr.2016.10.007>.
- [3] L. Yu, B.Y. Xia, X. Wang, X.W. Lou, General formation of M-MoS₃ (M = Co, Ni) hollow structures with enhanced electrocatalytic activity for hydrogen evolution, *Adv. Mater.* 28 (2016) 92–97, <https://doi.org/10.1002/adma.201504024>.
- [4] L. Zhang, H.B. Wu, Y. Yan, X. Wang, X.W. (David) Lou, Hierarchical MoS₂ micro-boxes constructed by nanosheets with enhanced electrochemical properties for lithium storage and water splitting, *Energy Environ. Sci.* 7 (2014) 3302–3306, <https://doi.org/10.1039/C4EE01932F>.
- [5] J. Deng, H. Li, S. Wang, D. Ding, M. Chen, C. Liu, Z. Tian, K.S. Novoselov, C. Ma, D. Deng, X. Bao, Multiscale structural and electronic control of molybdenum disulfide foam for highly efficient hydrogen production, *Nat. Commun.* 8 (2017) 14430, <https://doi.org/10.1038/ncomms14430>.
- [6] Y. Luo, L. Tang, U. Khan, Q. Yu, H.-M. Cheng, X. Zou, B. Liu, Morphology and surface chemistry engineering toward pH-universal catalysts for hydrogen evolution at high current density, *Nat. Commun.* 10 (2019), <https://doi.org/10.1038/s41467-018-07792-9>.
- [7] J. Di, C. Yan, A.D. Handoko, Z.W. Seh, H. Li, Z. Liu, Ultrathin two-dimensional materials for photo- and electrocatalytic hydrogen evolution, *Mat. Today* 21 (2018) 749–770, <https://doi.org/10.1016/j.mattod.2018.01.034>.
- [8] Z. Hu, Z. Wu, C. Han, J. He, Z. Ni, W. Chen, Two-dimensional transition metal dichalcogenides: interface and defect engineering, *Chem. Soc. Rev.* 47 (2018) 3100–3128, <https://doi.org/10.1039/C8CS00024G>.
- [9] H. Lin, H. Li, Y. Li, J. Liu, X. Wang, L. Wang, Hierarchical CoS/MoS₂ and Co₃S₄/MoS₂/Ni₂P nanotubes for efficient electrocatalytic hydrogen evolution in alkaline media, *J. Mater. Chem. A Mater. Energy Sustain.* 5 (2017) 25410–25419, <https://doi.org/10.1039/C7TA06080K>.

doi.org/10.1039/C7TA08760H.

[10] J.D. Wiensch, J. John, J.M. Velazquez, D.A. Torelli, A.P. Pieterick, M.T. McDowell, K. Sun, X. Zhao, B.S. Brunschwig, N.S. Lewis, Comparative Study in Acidic and Alkaline Media of the Effects of pH and Crystallinity on the Hydrogen-Evolution Reaction on MoS₂ and MoSe₂, *ACS Energy Lett.* 2 (2017) 2234–2238, <https://doi.org/10.1021/acsenergylett.7b00700>.

[11] Z. Zhai, C. Li, L. Zhang, H.-C. Wu, L. Zhang, N. Tang, W. Wang, J. Gong, Dimensional construction and morphological tuning of heterogeneous MoS₂/NiS electrocatalysts for efficient overall water splitting, *J. Mater. Chem. A Mater. Energy Sustain.* 6 (2018) 9833–9838, <https://doi.org/10.1039/C8TA03304H>.

[12] X.F. Lu, L. Yu, X.W.(David) Lou, Highly crystalline Ni-doped FeP/carbon hollow nanorods as all-pH efficient and durable hydrogen evolving electrocatalysts, *Sci. Adv.* 5 (2019) eaav6009, <https://doi.org/10.1126/sciadv.aav6009>.

[13] H. Li, C. Tsai, A.L. Koh, L. Cai, A.W. Contrynman, A.H. Fragapane, J. Zhao, H.S. Han, H.C. Manoharan, F. Abild-Pedersen, J.K. Norskov, X. Zheng, Activating and optimizing MoS₂ basal planes for hydrogen evolution through the formation of strained sulphur vacancies, *Nat. Mater.* 15 (2016), <https://doi.org/10.1038/nmat4564> 364–364.

[14] H. Wang, L. Ouyang, G. Zou, C. Sun, J. Hu, X. Xiao, L. Gao, Optimizing MoS₂ Edges by Alloying Ivalent W for Robust Hydrogen Evolution Activity, *ACS Catal.* 8 (2018) 9529–9536, <https://doi.org/10.1021/acscatal.8b02162>.

[15] S. Park, J. Park, H. Abroshan, L. Zhang, J.K. Kim, J. Zhang, J. Guo, S. Siahrostami, X. Zheng, Enhancing catalytic activity of MoS₂ basal plane S-Vacancy by Co cluster addition, *ACS Energy Lett.* 3 (2018) 2685–2693, <https://doi.org/10.1021/acsenergylett.8b01567>.

[16] P. Xiong, R. Ma, N. Sakai, L. Nurdwijayanto, T. Sasaki, Unilamellar metallic MoS₂/Graphene superlattice for efficient sodium storage and hydrogen evolution, *ACS Energy Lett.* 3 (2018) 997–1005, <https://doi.org/10.1021/acsenergylett.8b00110>.

[17] D. Escalera-López, Z. Lou, N.V. Rees, Benchmarking the activity, stability, and inherent electrochemistry of amorphous molybdenum sulfide for hydrogen production, *Adv. Energy Mater.* 9 (2019) 1802614, , <https://doi.org/10.1002/aenm.201802614>.

[18] H. Zhang, L. Yu, T. Chen, W. Zhou, X.W.D. Lou, Surface modulation of hierarchical MoS₂ nanosheets by Ni single atoms for enhanced electrocatalytic hydrogen evolution, *Adv. Funct. Mater.* 28 (2018) 1807086, , <https://doi.org/10.1002/adfm.201807086>.

[19] W. Wu, C. Niu, C. Wei, Y. Jia, C. Li, Q. Xu, Activation of MoS₂ basal Planes for hydrogen evolution by zinc, *Angew. Chemie Int. Ed. English* 58 (2019) 2029–2033, <https://doi.org/10.1002/anie.201812475>.

[20] M.A. Lukowski, A.S. Daniel, F. Meng, A. Forticaux, L. Li, S. Jin, Enhanced Hydrogen Evolution Catalysis from Chemically Exfoliated Metallic MoS₂ Nanosheets, *J. Am. Chem. Soc.* 135 (2013) 10274–10277, <https://doi.org/10.1021/ja404523s>.

[21] Y. Yu, G.-H. Nam, Q. He, X.-J. Wu, K. Zhang, Z. Yang, J. Chen, Q. Ma, M. Zhao, Z. Liu, F.-R. Ran, X. Wang, H. Li, X. Huang, B. Li, Q. Xiong, Q. Zhang, Z. Liu, L. Gu, Y. Du, W. Huang, H. Zhang, High phase-purity 1T'-MoS₂- and 1T'-MoSe₂-layered crystals, *Nat. Chem.* 10 (2018) 638–643, <https://doi.org/10.1038/s41557-018-0035-6>.

[22] Y. Shi, Y. Zhou, D.-R. Yang, W.-X. Xu, C. Wang, F.-B. Wang, J.-J. Xu, X.-H. Xia, H.-Y. Chen, Energy level engineering of MoS₂ by transition-metal doping for accelerating hydrogen evolution reaction, *J. Am. Chem. Soc.* 139 (2017) 15479–15485, <https://doi.org/10.1021/jacs.7b08881>.

[23] D. Voiry, R. Fullon, J. Yang, C. de Carvalho Castro e Silva, R. Kappera, I. Bozkurt, D. Kaplan, M.J. Lagos, P.E. Batson, G. Gupta, A.D. Mohite, L. Dong, D. Er, V.B. Shenoy, T. Asefa, M. Chhowalla, The role of electronic coupling between substrate and 2D MoS₂ nanosheets in electrocatalytic production of hydrogen, *Nat. Mater.* 15 (2016) 1003–1009, <https://doi.org/10.1038/nmat4660>.

[24] L. Guo, C. Zhong, L. Shi, L. Ju, X. Wang, D. Yang, K. Bi, Y. Hao, Y. Yang, Phase and defect engineering of MoS₂ stabilized in periodic TiO₂ nanoporous film for enhanced solar water splitting, *Adv. Opt. Mater.* (2018) 1801403, <https://doi.org/10.1002/adom.201801403>.

[25] H. Yu, Y. Xue, L. Hui, C. Zhang, Y. Zhao, Z. Li, Y. Li, Controlled growth of MoS₂ nanosheets on 2D N-Doped graphdiyne nanolayers for highly associated effects on water reduction, *Adv. Funct. Mater.* 28 (2018) 1707564, , <https://doi.org/10.1002/adfm.201707564>.

[26] C. Tan, Z. Luo, A. Chaturvedi, Y. Cai, Y. Du, Y. Gong, Y. Huang, Z. Lai, X. Zhang, L. Zheng, X. Qi, M.H. Goh, J. Wang, S. Han, X.-J. Wu, L. Gu, C. Kloc, H. Zhang, Preparation of high-percentage 1T-Phase transition metal dichalcogenide nanodots for electrochemical hydrogen evolution, *Adv. Mater.* 30 (2018) 1705509, <https://doi.org/10.1002/adma.201705509>.

[27] M. Raju, A.C.T. van Duin, K.A. Fichthorn, Mechanisms of oriented attachment of TiO₂ nanocrystals in vacuum and humid environments: reactive molecular dynamics, *Nano Lett.* 14 (2014) 1836–1842, <https://doi.org/10.1021/nl404533k>.

[28] M.P. Boneschanscher, W.H. Evers, J.J. Geuchies, T. Altantzis, B. Goris, F.T. Rabouw, S.A.P. van Rossum, H.S.J. van der Zant, L.D.A. Siebbeles, G. Van Tendeloo, I. Swart, J. Hilhorst, A.V. Petukhov, S. Bals, D. Vanmaekelbergh, Long-range orientation and atomic attachment of nanocrystals in 2D honeycomb superlattices, *Science* 344 (2014) 1377–1380, <https://doi.org/10.1126/science.1252642>.

[29] D. Li, M.H. Nielsen, J.R.I. Lee, C. Frandsen, J.F. Banfield, J.J. De Yoreo, Direction-specific interactions control crystal growth by oriented attachment, *Science* 336 (2012) 1014–1018, <https://doi.org/10.1126/science.1219643>.

[30] M.A.R. Anjum, H.Y. Jeong, M.H. Lee, H.S. Shin, J.S. Lee, Efficient hydrogen evolution reaction catalysis in alkaline media by all-in-One MoS₂ with multifunctional active sites, *Adv. Mater.* 30 (2018) 1707105, <https://doi.org/10.1002/adma.201707105>.

[31] J. Zhu, Z.-C. Wang, H. Dai, Q. Wang, R. Yang, H. Yu, M. Liao, J. Zhang, W. Chen, Z. Wei, N. Li, L. Du, D. Shi, W. Wang, L. Zhang, Y. Jiang, G. Zhang, Boundary activated hydrogen evolution reaction on monolayer MoS₂, *Nat. Commun.* 10 (2019), <https://doi.org/10.1038/s41467-019-10269-9>.

[32] G. Liu, A.W. Robertson, M.M.-J. Li, W.C.H. Kuo, M.T. Darby, M.H. Muhieddine, Y.-C. Lin, K. Suenaga, M. Stamatakis, J.H. Warner, S.C.E. Tsang, MoS₂ monolayer catalyst doped with isolated Co atoms for the hydrodeoxygenation reaction, *Nat. Chem.* 9 (2017) 810–816, <https://doi.org/10.1038/nchem.2740>.

[33] Q. Xu, Y. Liu, H. Jiang, Y. Hu, H. Liu, C. Li, Unsaturated sulfur edge engineering of strongly coupled MoS₂ nanosheet-carbon macroporous hybrid catalyst for enhanced hydrogen generation, *Adv. Energy Mater.* 9 (2019) 1802553, , <https://doi.org/10.1002/aenm.201802553>.

[34] L.-B. Huang, L. Zhao, Y. Zhang, Y.-Y. Chen, Q.-H. Zhang, H. Luo, X. Zhang, T. Tang, L. Gu, J.-S. Hu, Self-limited on-site conversion of MoO₃ nanodots into vertically aligned ultrasmall monolayer MoS₂ for efficient hydrogen evolution, *Adv. Energy Mater.* 8 (2018) 1800734, <https://doi.org/10.1002/aenm.201800734>.

[35] J. Zhang, C. Zhang, Z. Wang, J. Zhu, Z. Wen, X. Zhao, X. Zhang, J. Xu, Z. Lu, Synergistic interlayer and defect engineering in VS₂ nanosheets toward efficient electrocatalytic hydrogen evolution reaction, *Small* 14 (2018) 1703098, , <https://doi.org/10.1002/smll.201703098>.

[36] X. Fan, Y. Liu, S. Chen, J. Shi, J. Wang, A. Fan, W. Zan, S. Li, W.A. Goddard, X.-M. Zhang, Defect-enriched iron fluoride-oxide nanoporous thin films bifunctional catalyst for water splitting, *Nat. Commun.* 9 (2018), <https://doi.org/10.1038/s41467-018-04248-y>.

[37] X. Li, T. Li, Y. Ma, Q. Wei, W. Qiu, H. Guo, X. Shi, P. Zhang, A.M. Asiri, L. Chen, B. Tang, X. Sun, Boosted electrocatalytic N₂ reduction to NH₃ by Defect-Rich MoS₂ nanoflower, *Adv. Energy Mater.* 8 (2018) 1801357, , <https://doi.org/10.1002/aenm.201801357>.

[38] M.A. Pimenta, E.D. Corro, B.R. Carvalho, C. Fantini, L.M. Malard, Comparative study of raman spectroscopy in graphene and MoS₂-type transition metal dichalcogenides, *Acc. Chem. Res.* 48 (2015) 41–47, <https://doi.org/10.1021/ar500280m>.

[39] J. Wang, J. Liu, D. Chao, J. Yan, J. Lin, Z.X. Shen, Self-assembly of honeycomb-like MoS₂ nanoarchitectures anchored into graphene foam for enhanced lithium-ion storage, *Adv. Mater.* 26 (2014) 7162–7169, <https://doi.org/10.1002/adma.201402728>.

[40] Q. Xiang, J. Yu, M. Jaroniec, Synergetic effect of MoS₂ and graphene as cocatalysts for enhanced photocatalytic H₂ production activity of TiO₂ nanoparticles, *J. Am. Chem. Soc.* 134 (2012) 6575–6578, <https://doi.org/10.1021/ja302846n>.

[41] L. Liao, S. Wang, J. Xiao, X. Bian, Y. Zhang, M.D. Scanlon, X. Hu, Y. Tang, B. Liu, H.H. Girault, A nanoporous molybdenum carbide nanowire as an electrocatalyst for hydrogen evolution reaction, *Energy Environ. Sci.* 7 (2014) 387–392, <https://doi.org/10.1039/C3EE42441C>.